Synergistic block of SARS-CoV-2 infection by combined drug inhibition of the host entry factors PIKfyve kinase and TMPRSS2 protease

Alex J.B. Kreutzberger[a,b], Anwesha Sanyal[a,b], Ravi Ojha[c], Jesse D. Pyle[d], Olli Vapalahti[c,e,f], Giuseppe Balistreri[c,e] and Tom Kirchhausen[a,b,g,#]

[a] Department of Cell Biology, Harvard Medical School, 200 Longwood Av, Boston, MA 02115, USA

[b] Program in Cellular and Molecular Medicine, Boston Children's Hospital, 200 Longwood Av, Boston, MA 02115, USA

[c] Department of Virology, Faculty of Medicine, University of Helsinki, Helsinki, Finland

[d] Program in Virology, Harvard Medical School, 200 Longwood Ave, Boston, MA 02115, USA

[e] Department of Veterinary Biosciences, University of Helsinki, Helsinki, Finland

[f] Virology and Immunology, Helsinki University Hospital Diagnostic Center (HUSLAB), Helsinki, Finland

[g] Department of Pediatrics, Harvard Medical School, 200 Longwood Ave, Boston, MA 02115, USA

Running Head: Synergistic block of SARS-CoV-2 infection

#Address correspondence to Tom Kirchhausen kirchhausen@crystal.harvard.edu

ABSTRACT

Repurposing FDA-approved inhibitors able to prevent infection by severe acute respiratory syndrome coronavirus 2 (SARS-CoV-2) could provide a rapid path to establish new therapeutic options to mitigate the effects of coronavirus disease 2019 (COVID-19). Proteolytic cleavages of the spike S protein of SARS-CoV-2, mediated by the host cell proteases cathepsin and TMPRSS2, alone or in combination, are key early activation steps required for efficient infection. The PIKfyve kinase inhibitor apilimod interferes with late endosomal viral traffic, and through an ill-defined mechanism prevents *in vitro* infection through late endosomes mediated by cathepsin. Similarly, inhibition of TMPRSS2 protease activity by camostat mesylate or nafamostat mesylate prevents infection mediated by the TMPRSS2-dependent and cathepsin-independent pathway. Here, we combined the use of apilimod with camostat mesylate or nafamostat mesylate and found an unexpected ~5-10-fold increase in their effectiveness to prevent SARS-CoV-2 infection in different cell types. Comparable synergism was observed using both, a chimeric vesicular stomatitis virus (VSV) containing S of SARS-CoV-2 (VSV-SARS-CoV-2) and SARS-CoV-2 virus. The substantial ~5-fold or more decrease of half maximal effective concentrations (EC_{50} values) suggests a plausible treatment strategy based on the combined use of these inhibitors.

IMPORTANCE

Infection by severe acute respiratory syndrome coronavirus 2 (SARS-CoV-2) is causing the coronavirus disease 2019 (COVID-2019) global pandemic. There are ongoing efforts to uncover effective antiviral agents that could mitigate the severity of the

disease by controlling the ensuing viral replication. Promising candidates include small molecules that inhibit the enzymatic activities of host proteins, thus preventing SARS-CoV-2 entry and infection. They include Apilimod, an inhibitor of PIKfyve kinase and camostat mesylate and nafamostat mesylate, inhibitors of TMPRSS2 protease. Our research is significant for having uncovered an unexpected synergism in the effective inhibitory activity of apilimod used together with camostat mesylate or with nafamostat mesylate.

54 **INTRODUCTION**

55 Severe acute respiratory syndrome coronavirus 2 (SARS-CoV-2) infection has caused
56 the global pandemic known as coronavirus disease 2019 (COVID-2019). Currently
57 there is no widespread use of an antiviral agent against the disease, but several
58 candidates have been identified (1-6). Apilimod is currently in a clinical trial for the
59 prevention of SARS-CoV-2 infections in the United States of America (ClinicalTrails.gov
60 Identifier: NCT04446377). The TMPRSS2 protease inhibitor camostat mesylate has
61 been tested with hospitalized COVID-19 patients in Denmark (7) and is in a clinical trial
62 on adult COVID-19 patients in France (ClinicalTrails.gov Identifier: NCT04608266),
63 while the higher affinity TMPRSS2 protease inhibitor, nafamostat mesylate, is being
64 used in COVID-19 related trials in Russia (ClinicalTrials.gov Identifier: NCT04623021),
65 South Korea (ClinicalTrails.gov Identifier: NCT04418128) and Japan (8).
66

67 Targeting the entry route of SARS-CoV-2 has been particularly challenging because
68 there appear to be at least two different pathways for virus entry into cells (1). SARS-
69 CoV-2 entry is mediated by the virus spike protein (9-11) and requires the receptor
70 ACE2 in the host cell (1, 12, 13). Upon engagement of the ACE2 receptor, the spike
71 protein catalyzes fusion of the viral membrane envelope with a host cell membrane to
72 release the contents of the virus into the cytoplasm of host cells. For the spike protein
73 to facilitate this reaction, it must first be cleaved by a host cell protease (1, 10). This
74 can be accomplished by different host proteases including TMPRSS2 and TMPRSS4
75 (14), Factor Xa (15, 16), and by cathepsins during endocytosis (1). The protease
76 inhibitors E-64 and camostat mesylate target cathepsin and TMPRSS2 and inhibit

77 SARS-CoV-2 infection (1), but their low (micromolar) affinities have made them unlikely
78 candidates for clinical use. Nafamostat mesylate inhibits TMPRSS2 with a high
79 (nanomolar) affinity (2, 6). Apilimod has been shown to function in the endosomal
80 pathway by inhibiting PIKfyve kinase causing a defect in viral trafficking prior to entry (3)
81 but how this relates to the cathepsin or TMPRSS2 protease dependent pathways has
82 not been investigated.
83
84 Using a chimeric vesicular stomatitis virus (VSV) in which the attachment and fusion
85 glycoprotein G is replaced by the spike S protein of SARS-CoV-2 (VSV-SARS-CoV-2)
86 (17) we investigate inhibition of infection in different cell types known to contain different
87 levels of cathepsin and TMPRSS2 proteases. We tested combinations of the protease
88 inhibitors E-64 (cathepsin), camostat mesylate and nafamostat mesylate (TMPRSS2)
89 and the lipid kinase inhibitor apilimod (PIKfyve kinase) on VSV-SARS-CoV-2 infection of
90 multiple cell types. We observed a 5-fold synergistic effect in the infection of VSV-
91 SARS-CoV-2 by simultaneous inhibition of TMPRSS2 and PIKfyve kinase. Furthermore,
92 the synergistic inhibitory effects on infection by VSV-SARS-CoV-2 or a clinical isolate of
93 SARS-CoV-2 were observed with nanomolar concentrations of camostat mesylate and
94 apilimod. This finding suggests that a combination of inhibitors that target two different
95 host factors in the entry pathway of SARS-CoV-2 will likely be more effective than
96 targeting either alone.

97 # RESULTS AND DISCUSSION
98
99 **VSV-SARS2-CoV-2 infection is partially prevented by PIKfyve kinase or TMPRSS2**
100 **protease inhibitors**
101 It has been proposed that two distinct host proteases, TMPRSS2 and cathepsin
102 facilitate different SARS2-CoV-2 viral entry routes - cell surface or endosomal - and
103 their abundance in different cell types may influence the entry pathway (1). To test this,
104 we employed a panel of inhibitors on SARS-CoV-2 infection in African green monkey
105 kidney epithelial derived VeroE6 cells poorly expressing TMPRSS2, VeroE6 cells stably
106 expressing ectopic TMPRSS2, as well as human colon carcinoma derived Caco-2 cells
107 and human lung derived Calu-3 cells naturally expressing TMPRSS2.
108
109 We first established the relative importance of the cathepsin-dependent route for
110 infection of VSV-SARS-CoV-2 by determining the effect of the cathepsin inhibitor E-64
111 on expression of eGFP mediated by VSV-SARS-CoV-2. As summarized in the plots in
112 Fig. 1A, we found a cell type dependence in the extent of infection block with a half
113 maximal effective concentration (EC_{50}) in the ~5-10 μM range. Notably, only Vero E6
114 cells treated with E-64 displayed a full infection block, the result expected for cells
115 expressing cathepsin but no TMPRSS2; in contrast, cells expressing cathepsin and
116 TMPRSS2 (VeroE6 + TMPRRS2, Caco-2) displayed a partial block, while Calu-3 cells
117 with minimal expression of cathepsin L (18) did not respond, as expected, to E-64
118 treatment (1).
119

120 We extended the analysis and studied the inhibitory effect by the PIKfyve kinase
121 inhibitor apilimod on VSV-SARS-CoV-2 infection (Fig. 1 B). We found that all cell types
122 shown to be sensitive to E-64 also responded to treatment with apilimod with EC_{50} ~ 10
123 nM whereas Calu-3, which is insensitive to E-64 (19), did not respond. Although
124 apilimod doesn't inhibit cathepsin B or L (20), these observations are consistent with
125 potential modulation of the endosomal availability of cathepsin by the activity of PIKfyve
126 kinase (21, 22).
127
128 A similar analysis, to document the reduction of viral infection using camostat mesylate
129 to block the protease activity of TPMRSS2 (Fig. 1C) or nafamostat mesylate (Fig. 1D)
130 showed, as anticipated, no response in Vero E6 cells lacking TMPRSS2, partial
131 inhibition in Vero E6 or Caco-2 cells expressing TMPRSS2 or full inhibition in Calu-3
132 cells naturally expressing TMPRSS2 but insensitive to cathepsin inhibition.
133
134 These observations are consistent with previous results (1, 2, 6, 19) that infection by
135 VSV-SARS-CoV-2 occurred through two complementary entry pathways with different
136 importance depending on the cell type, one depending on the proteolytic activity of
137 cathepsin and the second relying of the proteolytic activity of TMPRSS2. As a negative
138 control for these experiments, we included infection by the parental VSV (Fig. 1E),
139 whose ability to infect host cells is known to be independent of the enzymatic activities
140 of cathepsin, TMPRSS2, or PIKfyve kinase (1-4, 6). As expected, none of the inhibitors
141 for these enzymes influenced the extent of VSV infectivity in any of the cells used. From

142 these results we could also exclude potential cytotoxic effects by the compounds in the
143 concentration range used.
144
145 **Synergistic prevention of VSV-SARS2-CoV-2 infection by combined use of**
146 **PIKfyve kinase and TMPRSS2 protease inhibitors**
147 Since the cathepsin and TMPRSS2-dependent activation of SARS-CoV-2 correspond to
148 complementary entry pathways thought to act independent of each other, we expected
149 an additive inhibitory effect upon their simultaneous inhibition in cells that express both
150 proteases. Indeed, VSV-CoV-2 infection of Vero E6 cells expressing cathepsin and
151 TMPRSS2 (VeroE6 +TMPRSS2) were equally inhibited (EC_{50} ~ 2 μM) by camostat
152 mesylate in the absence or increasing concentrations of E-64 up to 20 μM, the
153 concentration at which E-64 maximally blocked VSV-CoV-2 infection (Fig. 2A). We used
154 SynergyFinder 2.0 (23) to compare the combined response obtained experimentally
155 with the expected outcome calculated by the Bliss synergy-scoring model. Using this
156 reference model, that considers multiplicative effect of single drugs as if they acted
157 independently (23, 24), we obtained an overall δ-score of 6 indicative of an additive
158 interaction between camostat and E-64. At combined high levels of camostat and E64,
159 these protease inhibitors also showed weak concentration dependence, consistent with
160 the prediction of a published model (25). In contrast, combined use of camostat
161 mesylate and apilimod led to enhanced inhibition of VSV-CoV-2 infection with a ~ 2-fold
162 decrease in the EC_{50} of camostat mesylate (from 1 to 0.4 μM) (Fig. 2B), suggestive of a
163 synergy effect.
164

165 We carried a similar set of experiments using Calu-3 cells known to be deficient in
166 Cathepsin-L (18, 26) and which are poorly susceptible to infection of filoviruses
167 mediated by the cathepsin-dependent infection route (18). These cells are insensitive to
168 inhibition by of VSV-SARS-CoV-2 and SARS-CoV-2 infection by E-64 (1, 19, 27, 28)
169 (Fig.1B) and apilimod ((19, 29), Fig. 1C). While presence of E-64 did not affect the
170 inhibition profile of camostat mesylate (Fig. 2C), we detected a ~ 5-fold decrease from 1
171 μM to 0.2 μM in the EC50 of apilimod in cells simultaneously treated with 10 μM E-64
172 (Fig. 2D). This result was unexpected, given that infection of the Calu-3 cells by SARS-
173 CoV-2 didn't appear to be affected by apilimod ((29) and Fig. 1C).
174
175 We extended the synergy analysis to verify the effects upon simultaneous use of
176 variable amounts of apilimod and nafamostat mesylate, another inhibitor of TMPRSS2.
177 Our data also indicates enhanced infection inhibition for nafamostat mesylate with a ~
178 20-fold decrease of EC_{50} from 0.02 to 0.001 μM (Fig. 3A, central panel). Simultaneous
179 treatment with apilimod and increasing amounts of nafamostat mesylate led to an
180 analogous enhanced potency of apilimod inhibition with a ~10-fold decrease of EC_{50}
181 from 0.01 to 0.001 μM (Fig. 3A, right panel). Formal evaluation for synergism using the
182 Bliss reference model was consistent with a synergy δ-score of 41 (a score greater than
183 10 indicates synergy (23)).
184
185 Comparable strong synergistic effects (δ-score of 34) by combined use of apilimod and
186 nafamostat mesylate were observed in Vero E6 cells expressing TMPRSS2 (Fig. 3B,
187 central and right panels) infected with VSV-SARS-CoV-2 D614G whose spike S protein

188 includes the point mutation known to increase infectivity of the native SARS-CoV-2 (30).
189 While this mutation has no effect on the virus entry mechanism or sensitivity to
190 proteases, it stabilizes the stalk region of the spike, which otherwise tend to fall apart
191 after furin cleavage between S1 and S2 (30-33).
192
193 Taken together, these synergy results highlight the unexpected non-additive
194 involvement of PIKfyve kinase activity for the functional effectiveness of TMPRSS2 to
195 mediate viral entry along the TMPRSS2 route.
196
197 **Synergistic prevention of SARS2-CoV-2 infection by combined use of PIKfyve**
198 **kinase and TMPRSS2 protease inhibitors**
199 To determine whether SARS-CoV-2 virus also display an enhanced block of infection
200 upon combined use of apilimod and camostat mesylate we infected Caco-2 cells
201 ectopically expressing hACE2, the main receptor for SARS-CoV-2. This cell line was
202 created as a way to enhance the susceptibility of Caco-2 to infection by SARS-CoV-2
203 since the parental cells express low endogenous levels of ACE2 (34); successful
204 infection was scored 18 hrs post infection by the appearance of viral N protein using
205 immunofluorescence microscopy (Fig. 4, left panel). The inhibitory EC_{50} of camostat
206 mesylate decreased ~ 6-fold from 0.6 to 0.1 μM when used together with apilimod, (Fig.
207 4, right panel). This observation extends our results from VSV-SARS-CoV-2 chimeras to
208 SARS-CoV-2 virus, and illustrates that combined chemical inhibition of PIKfyve kinase
209 and TMPRSS2 protease activities is likely to also prevent SARS-CoV-2 infection with
210 strong synergy.

211

212 ## Final remarks

213 According to our present understanding of early steps necessary for successful
214 infection, SARS-CoV-2 would enter cells using two main redundant routes, each
215 requiring cleavage of the viral S spike protein, one dependent on the proteolytic
216 activities of members of the cathepsin family, the other requiring proteolysis by
217 TMPRSS2 or similar transmembrane-serine proteases. Expression level of these
218 proteases depends on cell type and hence their relative importance to support
219 successful infection would hinge in part on their relative expression. Cathepsin is
220 primarily found in late endosomes or lysosomes and requires low pH for optimal
221 enzymatic activity; for these reasons it has been proposed that SARS-CoV-2 entry
222 occurs from the endolysosomal compartment (35, 36). In contrast, TMPRSS2 is thought
223 to be at the cell surface (37) and its optimal proteolytic activity is pH independent (38);
224 hence it has been inferred that TMPRSS2 cleavage of spike S protein occurs on virions
225 at the plasma membrane from which viral entry is then assumed to occur (1).
226
227 Not surprising for protease inhibitors with different targets, combined inhibition of the
228 enzymatic activities of cathepsin and TMPRSS2 by the respective protease inhibitors E-
229 64 and camostat mesylate led to additive prevention of infection by
230 SARS-CoV-2 (1) and by the VSV-SARS-CoV-2 chimera (this study).
231
232 Apilimod specifically inhibits PIKfyve kinase thereby blocking accumulation of PI(3,5)P2,
233 a key phosphoinositide required to modulate the function of a number of proteins

234 involved in late endosomal traffic (3, 21, 39, 40). While it is now well established that
235 interference with PIKfyve kinase prevents infection of a selected group of viruses
236 including Ebola (20), VSV-Ebola (3), Marburg (20), VSV-SARS-CoV-2 (3) and native
237 SARS-CoV-2 (3-5), the molecular mechanism events responsible for the interference
238 remain to be determined. It has been shown that Apilimod has anti-Ebola infection
239 synergy with clomiphene cytrate (δ-score of 23.8; re-calculated from data in Fig. 1B of
240 (41) using the Bliss reference model (23)) and also with other drugs that interfere, by
241 unknown mechanisms, with Ebola entry in late endosomes (41). We have now shown
242 synergistic inhibition of SARS-CoV-2 infection by combined use of apilimod and
243 camostat or apilimod and nafamostat mesylate, even in cells as diverse as Vero (which
244 have an active cathepsin entry pathway) and Calu-3 (which lack it).
245
246 Prevailing models for the cellular location of TMPRSS2-activated SARS-CoV-2 entry
247 favor fusion at the cell surface rather than from endosomal compartments, because
248 TMPRSS2 activity is pH independent. Ebola or SARS-CoV-2 viruses accumulate in
249 EEA1 containing early endosomes (3, 20), a behavior consistent with the disruption of
250 endolysosomal traffic that occurs when PIKfyve kinase activity is inhibited by genetic or
251 pharmacological means (21, 40, 42). It is therefore possible that changes in the
252 endosomal milieu, combined with redirection of SARS-CoV-2 and/or TMPRSS2 traffic in
253 the presence of apilimod, might make infection more dependent on TMPRSS2
254 pharmacological inactivation than in its absence. Combined presence of apilimod and
255 camostat or nafamostat mesylate would manifest as synergy of these compounds to
256 prevent infection. These observations would also be consistent with favored entry of

257 TMPRSS2-activated SARS-CoV-2 from internal membrane compartments rather than
258 from the cell surface.
259
260 The strong synergy we described in the laboratory setting for single cell types upon
261 combined use of the PIKfyve kinase and TMPRSS2 inhibitors highlights the potential
262 clinical advantage of using a similar strategy to ameliorate the viral load and potentially
263 reduce the risk to COVID-19 in patients infected with SARS-CoV-2 based on
264 simultaneous inhibition of these enzymes. Variants of apilimod and camostat, rendered
265 more soluble by mesylate modification, are currently in clinical trials as orally
266 administered inhibitors dispensed alone for various indications, including COVID-19 (7,
267 43, 44). More soluble nafamostat mesylate has been administered intravenously to
268 treat COVID-19 patients (8). We do not yet know how efficiently these inhibitors reach
269 nasopharyngeal and lung tissues; nevertheless, we surmise that combined use of these
270 PIKfyve and TMPRSS2 inhibitors might also recapitulate the ~5-10-fold increase in
271 inhibitor efficiency that we observe in the laboratory setting, offering considerable
272 advantage for clinical application.

273 **FIGURE LEGENDS**

274 **Fig. 1. Protease inhibitors E-64, apilimod, camostat mesylate or nafamostat**
275 **mesylate prevent infection by VSV-SARS-CoV-2 but not by VSV.**

276 **(A)** Schematic of infectivity assay for cells pretreated for 1 h or not with the inhibitors,
277 subsequently infected with VSV-SARS-CoV-2 for 1 h in the presence or absence of
278 inhibitors. The cells were incubated for another 7 h in the presence or absence of
279 inhibitors and then fixed; the percentage of cells expressing eGFP measured by
280 spinning disc confocal microscopy.

281 **(B-F)** Quantification of the number of infected cells from three independent experiments,
282 each determined from 5 fields of view containing 80-200 cells per experiment (error bars
283 show SEM) for the indicated cell types. Infected Vero **(B)** or Vero + TMPRSS2 cells **C**)
284 were analyzed 8 hpi using 0.5 μg/mL VSV-SARS-CoV-2 RNA. Infected Caco-2 **(D)** or
285 Calu-3 cells **(E**) were analyzed 8 hpi using 5 μg/mL VSV-SARS-CoV-2 RNA. Cells
286 infected with 0.075 μg/mL VSV RNA **(F)** were analyzed 6 hpi. In each case, these virus
287 concentrations and conditions of infection corresponded to an MOI of ~ 0.5.

288

289 **Fig. 2. Synergistic inhibition of VSV-SARS2-CoV-2 infection by combined use of**
290 **apilimod and camostat mesylate.**

291 Data are from infection results using VSV-SARS2-CoV-2 obtained with different cell
292 types in the absence or combined presence at increasing concentrations of E-64 and
293 camostat mesylate **(A, C)** or apilimod and camostat mesylate **(B, D)**. Representative
294 maximum-Z projections views (left panels) are from whole-cell volume images obtained
295 with optical sections separated by 0.5 μm using spinning disk confocal microscopy; cells

296 were infected with 0.5 μg/mL viral RNA VSV-SARS-CoV-2 and imaged 8 hpi. Scale
297 bar: 50 μm. Corresponding quantifications of infection (right panels) are shown in the
298 plots. Each point corresponds to one independent experiment; the data represent
299 results from 5 fields of view containing 80-200 cells per experiment. Estimated EC_{50}'s
300 are indicated. Significance in the difference of EC_{50} was determined from fitting
301 replicated experiments and using an unpaired t-test; P-values were 0.02 for **(B)** and
302 0.002 for **(D);** there was no statistically significant difference in the EC50 values for the
303 experiments reported in **(A)** or **(C)**.
304
305 **Fig. 3. Synergistic inhibition of VSV-SARS2-CoV-2 infection by combined use of**
306 **apilimod and nafamostat mesylate.**
307 Data are from infection results obtained with VeroE6 + TPRSS2 cells in the absence or
308 combined presence at increasing concentrations of apilimod and nafamostat mesylate.
309 Representative maximum-Z projections views (left panels) are from whole-cell volume
310 images obtained with optical sections separated by 0.5 μm using spinning disk confocal
311 microscopy; cells were infected with 0.5 μg/mL viral RNA VSV-SARS-CoV-2 **(A)** or 0.2
312 μg/mL VSV-SARS-CoV-2 D614G viral RNA **(B)** and imaged 8 hpi. Scale bar: 50 μm.
313 Corresponding quantifications of infection (right panels) are shown in the plots. Each
314 point corresponds to one independent experiment; the data represent results from 5
315 fields of view containing 80-200 cells per experiment. Estimated EC_{50}'s are indicated.
316 Both plots in the central and right panels used the same data.
317

318 **Fig. 4. Synergistic inhibition of SARS2-CoV-2 infection by combined use of**
319 **apilimod and camostat mesylate.**
320 Natural SARS-CoV-2 infection inhibition in Caco-2 + hACE2 cells (MOI = 0.5) by
321 camostat mesylate in the absence or combined presence of apilimod. Representative
322 examples of images of fixed samples stained with an antibody specific for N (red) and
323 with Hoechst DNA stain (cyan) to identify the nuclei obtained using wide field
324 epifluorescence microscopy (left panels) and corresponding quantifications of infection
325 (right panels) are shown. Each data points were from 4 independent experiments,
326 representing results from 6,000-10,000 cells per experiment. Estimated EC_{50}'s are
327 shown. Significance in the difference (P-value of 0.01) of EC_{50} was determined using an
328 unpaired t-test after a least square non-linear fitting of the data curves from replicated
329 experiments.

330 # MATERIAL AND METHODS

331 **Materials**

332 These reagents were purchased as indicated: Dulbecco modified Eagles Medium
333 (DMEM) supplemented with 4.5 g/L glucose, L-glutamine, and sodium pyruvate
334 (Corning, Inc., cat. 10-013-CV), fetal bovine serum (FBS, Atlanta Biologicals, cat.
335 S11150H), penicillin-streptomycin 100x solution (VWR, cat. 45000-652), camostat
336 mesylate (Sigma-Aldrich, cat. SML0057), E-64 (Santa Cruz Biotechnology, cat. sc-
337 201276), nafamostat mesylate (Cayman Chemical Company, cat. #14837), apilimod
338 (MedChem Express, cat. HY-14644), dimethyl sulfoxide (DMSO, Sigma-Aldrich, cat.
339 26855), Round cover glass #1.5, 25 mm (Cellvis cat. C8-1.5H-N), Polydimethylsiloxane
340 (PDMS, SYLGARD from Krayden, cat. DC4019862), isopropyl alcohol (VWR, cat. 9080-
341 03/MK303108), potassium hydroxide (Sigma-Aldrich, cat. 484016), wheat germ
342 agglutinin (WGA)-Alexa647 (Invitrogen, cat. W32466), paraformaldehyde (Sigma-
343 Aldrich, cat. P6148), sodium phosphate dibasic (Thermo Fisher Scientific, cat. BP329-
344 1), potassium phosphate monobasic (Sigma-Aldrich, cat. P5379), sodium chloride (EMD
345 Millipore, cat. SX0420-5), and potassium chloride (Thermo Fisher Scientific, cat. P217-
346 500), TRIS (Goldbio, cat. T-400-500), EDTA (Sigma-Aldrich, cat. E5134), sucrose
347 (Sigma-Aldrich, cat. S0389), fetal calf serum (FCS, Hyclone, cat. SH30073.03), bovine
348 serum albumin (GE Healthcare), Triton-X (Thermo Fischer, cat. 28314), Hoechst DNA
349 stain (Thermo Fischer, cat. 62249), L-glutamine (Sigma, cat. G7513), Hoechst DNA dye
350 (cat. H6021, Sigma-Aldrich), and Alexa 647 fluorescently labelled goat anti-rabbit
351 antibody (Thermo Fisher, cat. A32733).

352

353 **Purification of VSV-SARS-CoV-2 chimeras**

354 Generation of recombinant VSV (Indiana serotype) expressing eGFP (VSV-eGFP) and
355 VSV-eGFP chimeras whose glycoprotein G was replaced with either the wild type spike
356 S protein of SARS-CoV-2 Wuhan-Hu-1 strain (VSV-SARS-CoV-2) or with the point
357 mutant D614G (VSV-SARS-CoV-2 D614G) was done as described (17). Briefly, VSV
358 was grown by infection of BSRT7/5 and VSV-SARS-CoV-2 chimeras were grown by
359 infection of MA104 cells. Cells were grown in 12-18 150 mm dishes and infected at an
360 MOI of 0.01. Virus-containing supernatant was collected at 48 hours post infection. The
361 supernatant was clarified by low-speed centrifugation at 1,000 × g for 10 min at room
362 temp. An initial pellet of virus and extracellular particles was generated by centrifugation
363 in a Ti45 fixed-angle rotor at 30,000 × g (25,000 rpm) for 2 hours at 4°C. The pellet was
364 resuspended overnight in 1X NTE (100 mM NaCl, 10 mM Tris-HCl pH 7.4, 1 mM EDTA)
365 at 4°C. The resuspended pellet was layered on top of a 15% sucrose-NTE cushion and
366 subjected to ultracentrifugation in a SW55 swinging bucket rotor at 110,000 × g (35,000
367 rpm) for 2 hours at 4°C. The supernatant was aspirated and virus pellet resuspended in
368 1X NTE overnight at 4°C. The resuspended virus pellet was separated on a 15-45%
369 sucrose-NTE gradient by ultracentrifugation in a SW55 swinging bucket rotor at 150,000
370 × g (40,000 rpm) for 1.5 hours at 4°C. The predominant light-scattering virus band was
371 observed in the lower third of the gradient and was extracted by side puncture of the
372 gradient tube. Extracted virus was diluted in 1X NTE and collected by ultracentrifugation
373 in a Ti60 fixed-angle rotor at 115,000 × g (40,000 rpm) for 2 hours at 4°C. The final
374 pellet was re-suspended overnight in 1X NTE in a volume of 0.2 to 0.5 mL depending
375 on the size of the pellet and stored at 4°C for use in subsequent imaging experiments.

376

377 **Isolation and propagation of SARS-CoV-2**

378 Human samples were obtained under the Helsinki University Hospital laboratory
379 research permit 30 HUS/32/2018 § 16. Isolation of SARS-CoV-2 from a COVID-19
380 Briefly, a nasopharyngeal swab in 500 µl of Copan UTM® Universal Transport Medium
381 was inoculated on Calu-3 cells (P1) and incubated for 1 h at 37°C, after which the
382 inoculum was removed and replaced with Minimum Essential Medium supplemented
383 with 2% FBS, L-glutamine, penicillin and streptomycin. Virus replication was determined
384 by RT-PCR for SARS-CoV-2 RdRP (45), and the infectious virus collected 48h after
385 inoculation. The P1 stock was propagated once (P2) in VeroE6+TMPRSS2, sequenced
386 and stored at -80 °C. Virus stocks were stored in DMEM, 2% FCS, 2 mM L-glutamine,
387 1% penicillin-streptomycin.

388

389 **Cell Culture**

390 VeroE6 (ATCC CRL-1586), Caco-2 (ATCC HTB-37), and Calu-3 cells (ATCC HTB-55)
391 were purchased from ATTC. VeroE6+TMPRSS2 cells were a gift from Siyan Ding (14).
392 VeroE6, VeroE6+TMPRSS2, Caco-2, and Calu-3 cells were maintained in DMEM
393 supplemented with 25 mM HEPES, pH 7.4, 10% fetal bovine serum and 1% penicillin-
394 streptomycin. VeroE6 and VeroE6+TMPRSS2 cells were grown at 37ºC and 5% CO_2
395 and split at a ratio of 1:10 every 3-4 days when cells were at ~90% confluency. Caco-2
396 cells were grown at 37ºC and 5% CO_2 and split at a ratio of 1:5 every 3-4 days when
397 cells were at ~95% confluency. Calu-3 cells were grown at 37ºC and 7% CO_2 and split
398 at a ratio of 1:3 every 5-6 days when cells were at ~95% confluency. BSR-T7 cells

399 were derived from BHC cells (46) and grown in DMEM supplemented with 10% FBS
400 and 1% penicillin-streptomycin. BSR-T7 were grown at 37°C and 5% CO_2 and split at a
401 ratio of 1:20 every 2-3 days when cells were at ~90% confluency. MA104 cells (ATCC,
402 CRL-2378.1) were grown in Media 199 supplemented with 10% FBS and 1% penicillin-
403 streptomycin. MA104 cells were grown at 37°C and 5% CO_2 and split at a ratio of 1:3
404 every 2 days when cells were at ~90% confluency. The media was changed in all cell
405 types every 2 days and regularly tested for presence of mycoplasma.
406
407 Caco-2 cells stably expressing human ACE2 were generated by transduction with third
408 generation lentivirus pLenti7.3/V5 DEST ACE2-EmGFP (prepared by the cloning facility
409 Dream-Lab, Institute of Biotechnology, University of Helsinki, Helsinki, Finland; the
410 expression of Emerald GFP is driven by the SV40 promoter. Cells expressing eGFP
411 were isolated by FACS. These cells were grown in DMEM media supplemented with
412 10% fetal calf serum, 1% penicillin-streptomycin, and 2 mM L-glutamine. Cells were
413 kept at 37°C, 5% CO_2, and split every 2-4 days when ~90% confluent.
414
415 **Infection protocol for VSV and VSV-SARS-CoV-2**
416 Polydimethylsiloxane was cured by vigorously mixing with curing reagent at a ratio of 1
417 to 10. PDMS was poured into 10 cm petri dish (5 g of PDMS per plate) and incubated
418 at 90 ^{o}C for ~4 hours. Plates were removed and stored at room temperature until use.
419 PDMS was removed from petri dish using a razor blade. 3 mm holes were punched into
420 PDMS which was cut with a blade to be ~6-10 mm. Glass slides were cleaned by
421 sonication first in isopropanol for 20 min then in 0.5M potassium hydroxide for 20 min

422 followed by extensive washing in Milli-q water. Glass was dried in an oven 60 ^{o}C for 30
423 minutes then bonded to the PDMS by exposing PDMS and glass to air plasma at 750
424 mTorr, 30 W for 2 minutes using a PDC-001 plasma cleaner (Harrick Plasma) then
425 firmly pressing glass and PDMS together. This was followed by placing bonded glass
426 and PDMS in an oven at 90 ^{o}C for 20 minutes. The glass cover slips mounted with a
427 PDMS well were then placed in 70% ethanol for 10 minutes to sterilize prior to use for
428 cell culture.
429
430 The day prior to the experiment cells were plated in PDMS wells on the glass slide
431 stored in a 6 well plate at a density to achieve ~70% confluence the day of the
432 experiment. On the day of the experiment cells were incubated with the desired
433 inhibitor concentration for 1 hour. Media was then removed and virus that had been
434 diluted into media containing the indicated inhibitor concentration was added to the well
435 in a volume of 10 μL. Media was left in the 6 well plate outside of the PDMS well at a
436 level less than the height of the PDMS well to maintain humidity and prevent
437 evaporation. After the virus was incubated with the cells for 1 hour the cells were
438 washed with media containing the indicated inhibitor and then the well was filled with
439 fresh media. In all experiment's cells were kept at 37°C and 5% (for Vero,
440 Vero+TMRPSS2, and Caco-2 cells) or 7% CO_2 (for Calu-3 cells) and media was pre
441 warmed to 37°C. At 6 hours after initiating the infection with VSV or 8 hours after
442 initiating the infection with VSV-SARS-CoV-2 media was removed and the cells were
443 stained by adding 5μg/mL WGA-Alexa647 in PBS (137 mM NaCl, 2.7 mM KCl, 8 mM
444 Na_2HPO_4, 2 mM KH_2PO_4, pH 7.4) for 30 seconds at room temperature. Cells were then

445 washed with sterile PBS 2 times and then fixed with 4% paraformaldehyde in PBS.
446 Infected cells were imaged using a spinning disk confocal microscope with a 40X oil
447 objective with a pixel size of 0.33 µm where 20 optical planes were taken at 0.5 µm
448 apart for every field of view (47). Cells were considered infected when they displayed a
449 cytosolic eGFP fluorescence signal with a relative intensity of 1.4 times that of the
450 background of uninfected cells. Example images are max intensity projections of the cell
451 volume where the outline (white) line was obtained by tracing the WGA-Alexa647 signal
452 outlining the cell.
453
454 **Infection protocol for SARS-CoV-2**
455 All experiments with SARS-CoV-2 were performed in BSL3 facilities at the University of
456 Helsinki with appropriate institutional permits. Virus samples were obtained under the
457 Helsinki University Hospital laboratory research permit 30 HUS/32/2018 § 16. Virus titers
458 were determined by plaque assay in VeroE6+TMPRSS2 cells. Cells in DMEM,
459 supplemented with 10% FBS, 2 mM L-glutamine, 1% penicillin-streptomycin, 20 mM
460 HEPES (pH 7.2 were seeded 48 h before treatment at a density of 15,000 cells per well
461 in 96-well imaging plates (PerkinElmer cat. 6005182). Inhibitors, or DMSO control, were
462 either added 60 min prior to infection, or added 90 min post infection at a multiplicity of
463 infection (MOI) 0.5 plaque forming units per cell. Infections were carried for 20 h at 37 °C
464 and 5% CO_2. Cells were then fixed with 4% paraformaldehyde in PBS for 30 min at room
465 temperature before being processed for immuno-detection of viral N protein, automated
466 fluorescence imaging and image analysis. Briefly, viral NP was detected with an in house
467 developed rabbit polyclonal antibody (34) counterstained with Alexa-647-conjugated goat

468 anti rabbit secondary antibody, and nuclear staining done using Hoechst DNA dye.
469 Automated fluorescence imaging was done using an epifluorescence high-content
470 Molecular Device Image-Xpress Nano microscope equipped with a 20x objective and a
471 4.7Mpixel CMOS camera (pixel size 0.332 μm). Image analysis was performed with the
472 software CellProfiler-3 (www.cellprofiler.org). Automated detection of nuclei was obtained
473 using the Otsu algorithm inbuilt in the software. To automatically identify infected cells,
474 an area surrounding each nucleus (5 pixels expansion of the nuclear area) was used to
475 estimate the fluorescence intensity of the viral NP immuno labeled protein, using an
476 intensity threshold such that less than 0.01% of positive cells were detected in non-
477 infected wells.
478
479 **Statistical analysis**
480 The significance of response (synergy δ-score) upon combined use of two drugs (Fig. 3)
481 was calculated using the Bliss reference model for combination of two drugs incorporated
482 in the stand-alone web-application SynergyFind v2 (23). This model assumes a stochastic
483 process in which the effects of two drugs act independently. δ-score values between -10
484 and 10 suggest an additive interaction; δ-scores larger than 10 suggest the interaction is
485 synergistic.
486
487 The $EC5_{50}$ values in Figures 2 B, C, and Figure 4 were obtained from replicate
488 determinations calculated with least-square nonlinear curve fitting using Igor Pro
489 (WaveMetrics). An unpaired T-test was then used to determine the statistical significance
490 in the difference in the values of EC_{50} of camostat mesylate as a function of apilimod.

491 **AUTHOR CONTRIBUTIONS**

492 We thank Sean Whelan for comments and suggestions. Alex J.B. Kreutzberger carried
493 out all the experiments in Figs. 1-3. Ravi Ojha and Giuseppe Balistreri carried out the
494 experiments in Fig. 4. Anwesha Sanyal maintained the cells lines and assisted with
495 infectivity assays. Ravi Ojha generated Caco2-ACE2+EmGFP cells and propagated
496 SARS-CoV-2 virus under the supervision of Olli Vapalahti. Jesse Pyle generated the
497 stocks of VSV-SARS-CoV-2 chimeras. We thank Tegy John Vadakkan for maintaining
498 the spinning disc confocal microscope. This research was supported by a NIH
499 Maximizing Investigators' Research Award (MIRA) GM130386, by research grants from
500 the Danish Technical University and SANA and unrestricted funds from IONIS to T.K;
501 Harvard Virology Program, NIH training Grant T32 AI07245 postdoctoral fellowship to
502 A.J.B.K.; by an Academy of Finland research grant 336490 by the Jane and Aatos
503 Erkko Foundation, by the EU Horizon 2020 program VEO 874735, and by Helsinki
504 University Hospital Funds TYH2018322 to O.V; by a research grant from the Academy
505 of Finland grant 318434 and private funds supporting COVID-19 research to G.B.; by
506 the University of Helsinki graduate program in Microbiology and Biotechnology to R.O.
507 Tom Kirchhausen and Alex J.B. Kreutzberger were responsible for the overall design of
508 the study; Tom Kirchhausen and Alex Kreutzberger drafted the manuscript; all authors
509 commented on the manuscript.

510 **REFERENCES**

511 1. Hoffmann M, Kleine-Weber H, Schroeder S, Kruger N, Herrler T, Erichsen S, Schiergens
512 TS, Herrler G, Wu NH, Nitsche A, Muller MA, Drosten C, Pohlmann S. 2020. SARS-
513 CoV-2 Cell Entry Depends on ACE2 and TMPRSS2 and Is Blocked by a Clinically
514 Proven Protease Inhibitor. Cell 181:271-280 e8.
515 2. Hoffmann M, Schroeder S, Kleine-Weber H, Muller MA, Drosten C, Pohlmann S. 2020.
516 Nafamostat Mesylate Blocks Activation of SARS-CoV-2: New Treatment Option for
517 COVID-19. Antimicrob Agents Chemother 64.
518 3. Kang YL, Chou YY, Rothlauf PW, Liu Z, Soh TK, Cureton D, Case JB, Chen RE,
519 Diamond MS, Whelan SPJ, Kirchhausen T. 2020. Inhibition of PIKfyve kinase prevents
520 infection by Zaire ebolavirus and SARS-CoV-2. Proc Natl Acad Sci U S A 117:20803-
521 20813.
522 4. Ou X, Liu Y, Lei X, Li P, Mi D, Ren L, Guo L, Guo R, Chen T, Hu J, Xiang Z, Mu Z,
523 Chen X, Chen J, Hu K, Jin Q, Wang J, Qian Z. 2020. Characterization of spike
524 glycoprotein of SARS-CoV-2 on virus entry and its immune cross-reactivity with SARS-
525 CoV. Nat Commun 11:1620.
526 5. Riva L, Yuan S, Yin X, Martin-Sancho L, Matsunaga N, Pache L, Burgstaller-
527 Muehlbacher S, De Jesus PD, Teriete P, Hull MV, Chang MW, Chan JF, Cao J, Poon
528 VK, Herbert KM, Cheng K, Nguyen TH, Rubanov A, Pu Y, Nguyen C, Choi A,
529 Rathnasinghe R, Schotsaert M, Miorin L, Dejosez M, Zwaka TP, Sit KY, Martinez-
530 Sobrido L, Liu WC, White KM, Chapman ME, Lendy EK, Glynne RJ, Albrecht R,
531 Ruppin E, Mesecar AD, Johnson JR, Benner C, Sun R, Schultz PG, Su AI, Garcia-Sastre
532 A, Chatterjee AK, Yuen KY, Chanda SK. 2020. Discovery of SARS-CoV-2 antiviral
533 drugs through large-scale compound repurposing. Nature 586:113-119.
534 6. Yamamoto M, Kiso M, Sakai-Tagawa Y, Iwatsuki-Horimoto K, Imai M, Takeda M,
535 Kinoshita N, Ohmagari N, Gohda J, Semba K, Matsuda Z, Kawaguchi Y, Kawaoka Y,
536 Inoue JI. 2020. The Anticoagulant Nafamostat Potently Inhibits SARS-CoV-2 S Protein-
537 Mediated Fusion in a Cell Fusion Assay System and Viral Infection In Vitro in a Cell-
538 Type-Dependent Manner. Viruses 12.
539 7. Gunst JD, Staerke NB, Pahus MH, Kristensen LH, Bodilsen J, Lohse N, Dalgaard LS,
540 Bronnum D, Frobert O, Honge B, Johansen IS, Monrad I, Erikstrup C, Rosendal R,
541 Vilstrup E, Mariager T, Bove DG, Offersen R, Shakar S, Cajander S, Jorgensen NP,
542 Sritharan SS, Breining P, Jespersen S, Mortensen KL, Jensen ML, Kolte L, Frattari GS,
543 Larsen CS, Storgaard M, Nielsen LP, Tolstrup M, Saedder EA, Ostergaard LJ, Ngo HTT,
544 Jensen MH, Hojen JF, Kjolby M, Sogaard OS. 2021. Efficacy of the TMPRSS2 inhibitor
545 camostat mesilate in patients hospitalized with Covid-19-a double-blind randomized
546 controlled trial. EClinicalMedicine doi:10.1016/j.eclinm.2021.100849:100849.
547 8. Doi K, Ikeda M, Hayase N, Moriya K, Morimura N, Group C-US. 2020. Nafamostat
548 mesylate treatment in combination with favipiravir for patients critically ill with Covid-
549 19: a case series. Crit Care 24:392.
550 9. Huang Y, Yang C, Xu XF, Xu W, Liu SW. 2020. Structural and functional properties of
551 SARS-CoV-2 spike protein: potential antivirus drug development for COVID-19. Acta
552 Pharmacol Sin 41:1141-1149.
553 10. Shang J, Wan Y, Luo C, Ye G, Geng Q, Auerbach A, Li F. 2020. Cell entry mechanisms
554 of SARS-CoV-2. Proc Natl Acad Sci U S A 117:11727-11734.

555 11. Wrapp D, Wang N, Corbett KS, Goldsmith JA, Hsieh CL, Abiona O, Graham BS,
556 McLellan JS. 2020. Cryo-EM structure of the 2019-nCoV spike in the prefusion
557 conformation. Science 367:1260-1263.
558 12. Yan R, Zhang Y, Li Y, Xia L, Guo Y, Zhou Q. 2020. Structural basis for the recognition
559 of SARS-CoV-2 by full-length human ACE2. Science 367:1444-1448.
560 13. Yang J, Petitjean SJL, Koehler M, Zhang Q, Dumitru AC, Chen W, Derclaye S, Vincent
561 SP, Soumillion P, Alsteens D. 2020. Molecular interaction and inhibition of SARS-CoV-
562 2 binding to the ACE2 receptor. Nat Commun 11:4541.
563 14. Zang R, Gomez Castro MF, McCune BT, Zeng Q, Rothlauf PW, Sonnek NM, Liu Z,
564 Brulois KF, Wang X, Greenberg HB, Diamond MS, Ciorba MA, Whelan SPJ, Ding S.
565 2020. TMPRSS2 and TMPRSS4 promote SARS-CoV-2 infection of human small
566 intestinal enterocytes. Sci Immunol 5.
567 15. Du L, Kao RY, Zhou Y, He Y, Zhao G, Wong C, Jiang S, Yuen KY, Jin DY, Zheng BJ.
568 2007. Cleavage of spike protein of SARS coronavirus by protease factor Xa is associated
569 with viral infectivity. Biochem Biophys Res Commun 359:174-9.
570 16. Frydman GH, Streiff MB, Connors JM, Piazza G. 2020. The Potential Role of
571 Coagulation Factor Xa in the Pathophysiology of COVID-19: A Role for Anticoagulants
572 as Multimodal Therapeutic Agents. TH Open 4:e288-e299.
573 17. Case JB, Rothlauf PW, Chen RE, Liu Z, Zhao H, Kim AS, Bloyet LM, Zeng Q, Tahan S,
574 Droit L, Ilagan MXG, Tartell MA, Amarasinghe G, Henderson JP, Miersch S, Ustav M,
575 Sidhu S, Virgin HW, Wang D, Ding S, Corti D, Theel ES, Fremont DH, Diamond MS,
576 Whelan SPJ. 2020. Neutralizing Antibody and Soluble ACE2 Inhibition of a Replication-
577 Competent VSV-SARS-CoV-2 and a Clinical Isolate of SARS-CoV-2. Cell Host
578 Microbe 28:475-485 e5.
579 18. Gonzalez-Hernandez M, Muller A, Hoenen T, Hoffmann M, Pohlmann S. 2019. Calu-
580 3cells are largely resistant to entry driven by filovirus glycoproteins and the entry defect
581 can be rescued by directed expression of DC-SIGN or cathepsin L. Virology 532:22-29.
582 19. Dittmar M, Lee JS, Whig K, Segrist E, Li M, Kamalia B, Castellana L, Ayyanathan K,
583 Cardenas-Diaz FL, Morrisey EE, Truitt R, Yang W, Jurado K, Samby K, Ramage H,
584 Schultz DC, Cherry S. 2021. Drug repurposing screens reveal cell-type-specific entry
585 pathways and FDA-approved drugs active against SARS-Cov-2. Cell Rep 35:108959.
586 20. Nelson EA, Dyall J, Hoenen T, Barnes AB, Zhou H, Liang JY, Michelotti J, Dewey WH,
587 DeWald LE, Bennett RS, Morris PJ, Guha R, Klumpp-Thomas C, McKnight C, Chen
588 YC, Xu X, Wang A, Hughes E, Martin S, Thomas C, Jahrling PB, Hensley LE, Olinger
589 GG, Jr., White JM. 2017. The phosphatidylinositol-3-phosphate 5-kinase inhibitor
590 apilimod blocks filoviral entry and infection. PLoS Negl Trop Dis 11:e0005540.
591 21. Baranov MV, Bianchi F, Schirmacher A, van Aart MAC, Maassen S, Muntjewerff EM,
592 Dingjan I, Ter Beest M, Verdoes M, Keyser SGL, Bertozzi CR, Diederichsen U, van den
593 Bogaart G. 2019. The Phosphoinositide Kinase PIKfyve Promotes Cathepsin-S-Mediated
594 Major Histocompatibility Complex Class II Antigen Presentation. iScience 11:160-177.
595 22. Gayle S, Landrette S, Beeharry N, Conrad C, Hernandez M, Beckett P, Ferguson SM,
596 Mandelkern T, Zheng M, Xu T, Rothberg J, Lichenstein H. 2017. Identification of
597 apilimod as a first-in-class PIKfyve kinase inhibitor for treatment of B-cell non-Hodgkin
598 lymphoma. Blood 129:1768-1778.
599 23. Ianevski A, Giri AK, Aittokallio T. 2020. SynergyFinder 2.0: visual analytics of multi-
600 drug combination synergies. Nucleic Acids Res 48:W488-W493.

601 24. Bliss C. 1939. The Toxicity Of Poisons Applied Jointly. Ann Appl Biol
602 doi:10.1111/j.1744-7348.1939.tb06990.x:585–615.
603 25. Padmanabhan P, Desikan R, Dixit NM. 2020. Targeting TMPRSS2 and Cathepsin B/L
604 together may be synergistic against SARS-CoV-2 infection. PLoS Comput Biol
605 16:e1008461.
606 26. Park JE, Li K, Barlan A, Fehr AR, Perlman S, McCray PB, Jr., Gallagher T. 2016.
607 Proteolytic processing of Middle East respiratory syndrome coronavirus spikes expands
608 virus tropism. Proc Natl Acad Sci U S A 113:12262-12267.
609 27. Murgolo N, Therien AG, Howell B, Klein D, Koeplinger K, Lieberman LA, Adam GC,
610 Flynn J, McKenna P, Swaminathan G, Hazuda DJ, Olsen DB. 2021. SARS-CoV-2
611 tropism, entry, replication, and propagation: Considerations for drug discovery and
612 development. PLoS Pathog 17:e1009225.
613 28. Mykytyn AZ, Breugem TI, Riesebosch S, Schipper D, van den Doel PB, Rottier RJ,
614 Lamers MM, Haagmans BL. 2021. SARS-CoV-2 entry into human airway organoids is
615 serine protease-mediated and facilitated by the multibasic cleavage site. Elife 10.
616 29. J K, Uckeley Z, P D, M S, S B, PY L. 2020. Host Cell Proteases Drive Early or Late
617 SARS-CoV-2 Penetration. bioRxiv doi:https://doi.org/10.1101/2020.12.22.423906.
618 30. Plante JA, Liu Y, Liu J, Xia H, Johnson BA, Lokugamage KG, Zhang X, Muruato AE,
619 Zou J, Fontes-Garfias CR, Mirchandani D, Scharton D, Bilello JP, Ku Z, An Z, Kalveram
620 B, Freiberg AN, Menachery VD, Xie X, Plante KS, Weaver SC, Shi PY. 2020. Spike
621 mutation D614G alters SARS-CoV-2 fitness. Nature doi:10.1038/s41586-020-2895-3.
622 31. Gobeil SM, Janowska K, McDowell S, Mansouri K, Parks R, Manne K, Stalls V, Kopp
623 MF, Henderson R, Edwards RJ, Haynes BF, Acharya P. 2021. D614G Mutation Alters
624 SARS-CoV-2 Spike Conformation and Enhances Protease Cleavage at the S1/S2
625 Junction. Cell Rep 34:108630.
626 32. Yurkovetskiy L, Wang X, Pascal KE, Tomkins-Tinch C, Nyalile TP, Wang Y, Baum A,
627 Diehl WE, Dauphin A, Carbone C, Veinotte K, Egri SB, Schaffner SF, Lemieux JE,
628 Munro JB, Rafique A, Barve A, Sabeti PC, Kyratsous CA, Dudkina NV, Shen K, Luban
629 J. 2020. Structural and Functional Analysis of the D614G SARS-CoV-2 Spike Protein
630 Variant. Cell 183:739-751 e8.
631 33. Zhang L, Jackson CB, Mou H, Ojha A, Peng H, Quinlan BD, Rangarajan ES, Pan A,
632 Vanderheiden A, Suthar MS, Li W, Izard T, Rader C, Farzan M, Choe H. 2020. SARS-
633 CoV-2 spike-protein D614G mutation increases virion spike density and infectivity. Nat
634 Commun 11:6013.
635 34. Cantuti-Castelvetri L, Ojha R, Pedro LD, Djannatian M, Franz J, Kuivanen S, van der
636 Meer F, Kallio K, Kaya T, Anastasina M, Smura T, Levanov L, Szirovicza L, Tobi A,
637 Kallio-Kokko H, Osterlund P, Joensuu M, Meunier FA, Butcher SJ, Winkler MS,
638 Mollenhauer B, Helenius A, Gokce O, Teesalu T, Hepojoki J, Vapalahti O, Stadelmann
639 C, Balistreri G, Simons M. 2020. Neuropilin-1 facilitates SARS-CoV-2 cell entry and
640 infectivity. Science 370:856-860.
641 35. Bayati A, Kumar R, Francis V, McPherson PS. 2021. SARS-CoV-2 infects cells
642 following viral entry via clathrin-mediated endocytosis. J Biol Chem
643 doi:10.1016/j.jbc.2021.100306:100306.
644 36. Khan N, Chen X, Geiger JD. 2020. Role of Endolysosomes in Severe Acute Respiratory
645 Syndrome Coronavirus-2 Infection and Coronavirus Disease 2019 Pathogenesis:
646 Implications for Potential Treatments. Front Pharmacol 11:595888.

647 37. Uhlen M, Fagerberg L, Hallstrom BM, Lindskog C, Oksvold P, Mardinoglu A,
648 Sivertsson A, Kampf C, Sjostedt E, Asplund A, Olsson I, Edlund K, Lundberg E, Navani
649 S, Szigyarto CA, Odeberg J, Djureinovic D, Takanen JO, Hober S, Alm T, Edqvist PH,
650 Berling H, Tegel H, Mulder J, Rockberg J, Nilsson P, Schwenk JM, Hamsten M, von
651 Feilitzen K, Forsberg M, Persson L, Johansson F, Zwahlen M, von Heijne G, Nielsen J,
652 Ponten F. 2015. Proteomics. Tissue-based map of the human proteome. Science
653 347:1260419.
654 38. Glowacka I, Bertram S, Muller MA, Allen P, Soilleux E, Pfefferle S, Steffen I, Tsegaye
655 TS, He Y, Gnirss K, Niemeyer D, Schneider H, Drosten C, Pohlmann S. 2011. Evidence
656 that TMPRSS2 activates the severe acute respiratory syndrome coronavirus spike protein
657 for membrane fusion and reduces viral control by the humoral immune response. J Virol
658 85:4122-34.
659 39. de Lartigue J, Polson H, Feldman M, Shokat K, Tooze SA, Urbe S, Clague MJ. 2009.
660 PIKfyve regulation of endosome-linked pathways. Traffic 10:883-93.
661 40. Kim GH, Dayam RM, Prashar A, Terebiznik M, Botelho RJ. 2014. PIKfyve inhibition
662 interferes with phagosome and endosome maturation in macrophages. Traffic 15:1143-
663 63.
664 41. Dyall J, Nelson EA, DeWald LE, Guha R, Hart BJ, Zhou H, Postnikova E, Logue J,
665 Vargas WM, Gross R, Michelotti J, Deiuliis N, Bennett RS, Crozier I, Holbrook MR,
666 Morris PJ, Klumpp-Thomas C, McKnight C, Mierzwa T, Shinn P, Glass PJ, Johansen
667 LM, Jahrling PB, Hensley LE, Olinger GG, Jr., Thomas C, White JM. 2018.
668 Identification of Combinations of Approved Drugs With Synergistic Activity Against
669 Ebola Virus in Cell Cultures. J Infect Dis 218:S672-S678.
670 42. Soares AC, Ferreira A, Marien J, Delay C, Lee E, Trojanowski JQ, Moechars D, Annaert
671 W, De Muynck L. 2021. PIKfyve activity is required for lysosomal trafficking of tau
672 aggregates and tau seeding. J Biol Chem 296:100636.
673 43. Billich A. 2007. Drug evaluation: apilimod, an oral IL-12/IL-23 inhibitor for the
674 treatment of autoimmune diseases and common variable immunodeficiency. IDrugs
675 10:53-9.
676 44. Uno Y. 2020. Camostat mesilate therapy for COVID-19. Intern Emerg Med 15:1577-
677 1578.
678 45. Corman VM, Landt O, Kaiser M, Molenkamp R, Meijer A, Chu DK, Bleicker T, Brunink
679 S, Schneider J, Schmidt ML, Mulders DG, Haagmans BL, van der Veer B, van den Brink
680 S, Wijsman L, Goderski G, Romette JL, Ellis J, Zambon M, Peiris M, Goossens H,
681 Reusken C, Koopmans MP, Drosten C. 2020. Detection of 2019 novel coronavirus
682 (2019-nCoV) by real-time RT-PCR. Euro Surveill 25.
683 46. Buchholz UJ, Finke S, Conzelmann KK. 1999. Generation of bovine respiratory syncytial
684 virus (BRSV) from cDNA: BRSV NS2 is not essential for virus replication in tissue
685 culture, and the human RSV leader region acts as a functional BRSV genome promoter. J
686 Virol 73:251-9.
687 47. Cocucci E, Aguet F, Boulant S, Kirchhausen T. 2012. The first five seconds in the life of
688 a clathrin-coated pit. Cell 150:495-507.
689

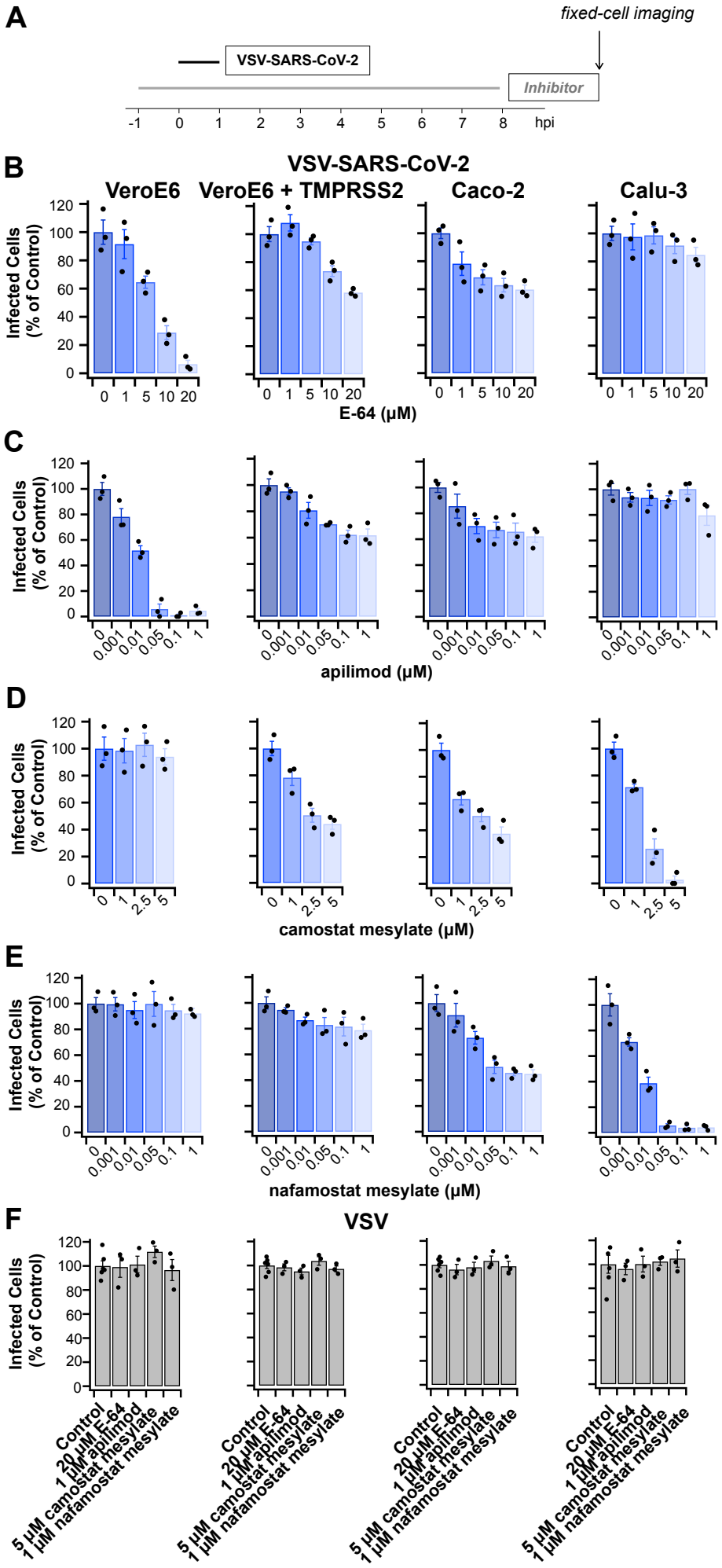
A
fixed-cell imaging
VSV-SARS-CoV-2
Inhibitor
-1 0 1 2 3 4 5 6 7 8 hpi
B
VSV-SARS-CoV-2
VeroE6
VeroE6 + TMPRSS2
Caco-2
Calu-3
Infected Cells (% of Control)
0 1 5 10 20
E-64 (μM)
C
0 0.001 0.01 0.05 0.1 1
apilimod (μM)
D
0 1 2.5 5
camostat mesylate (μM)
E
nafamostat mesylate (μM)
F
VSV
Control
20 μM E-64
1 μM apilimod
5 μM camostat mesylate
1 μM nafamostat mesylate

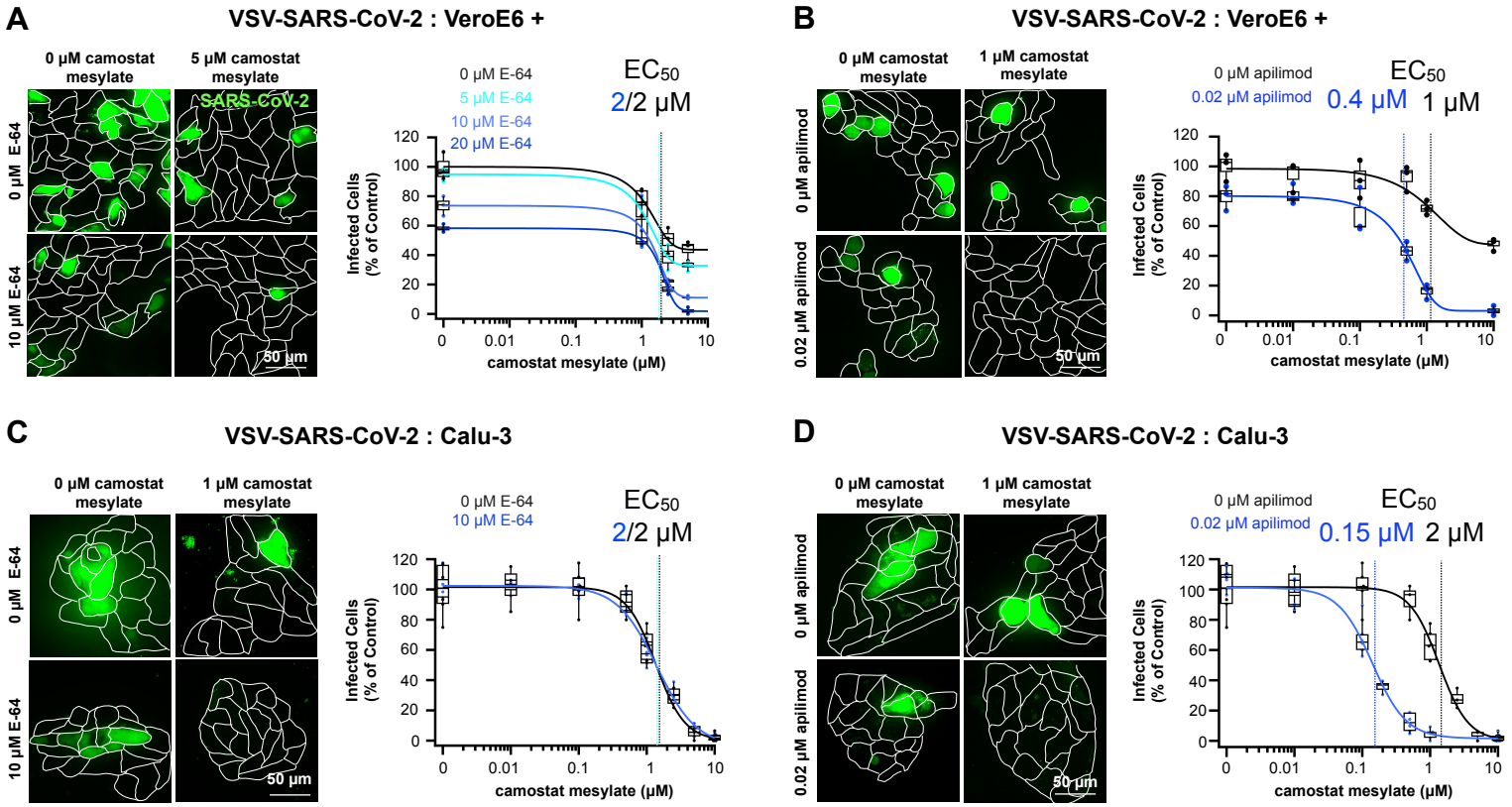
A
VSV-SARS-CoV-2 : VeroE6 +
0 µM camostat mesylate
5 µM camostat mesylate
0 µM E-64
10 µM E-64
SARS-CoV-2
50 µm
0 µM E-64
5 µM E-64
10 µM E-64
20 µM E-64
EC50
2/2 µM
Infected Cells (% of Control)
camostat mesylate (µM)
B
VSV-SARS-CoV-2 : VeroE6 +
0 µM camostat mesylate
1 µM camostat mesylate
0 µM apilimod
0.02 µM apilimod
50 µm
0 µM apilimod
0.02 µM apilimod
EC50
0.4 µM
1 µM
Infected Cells (% of Control)
camostat mesylate (µM)
C
VSV-SARS-CoV-2 : Calu-3
0 µM camostat mesylate
1 µM camostat mesylate
0 µM E-64
10 µM E-64
50 µm
0 µM E-64
10 µM E-64
EC50
2/2 µM
Infected Cells (% of Control)
camostat mesylate (µM)
D
VSV-SARS-CoV-2 : Calu-3
0 µM camostat mesylate
1 µM camostat mesylate
0 µM apilimod
0.02 µM apilimod
50 µm
0 µM apilimod
0.02 µM apilimod
EC50
0.15 µM
2 µM
Infected Cells (% of Control)
camostat mesylate (µM)

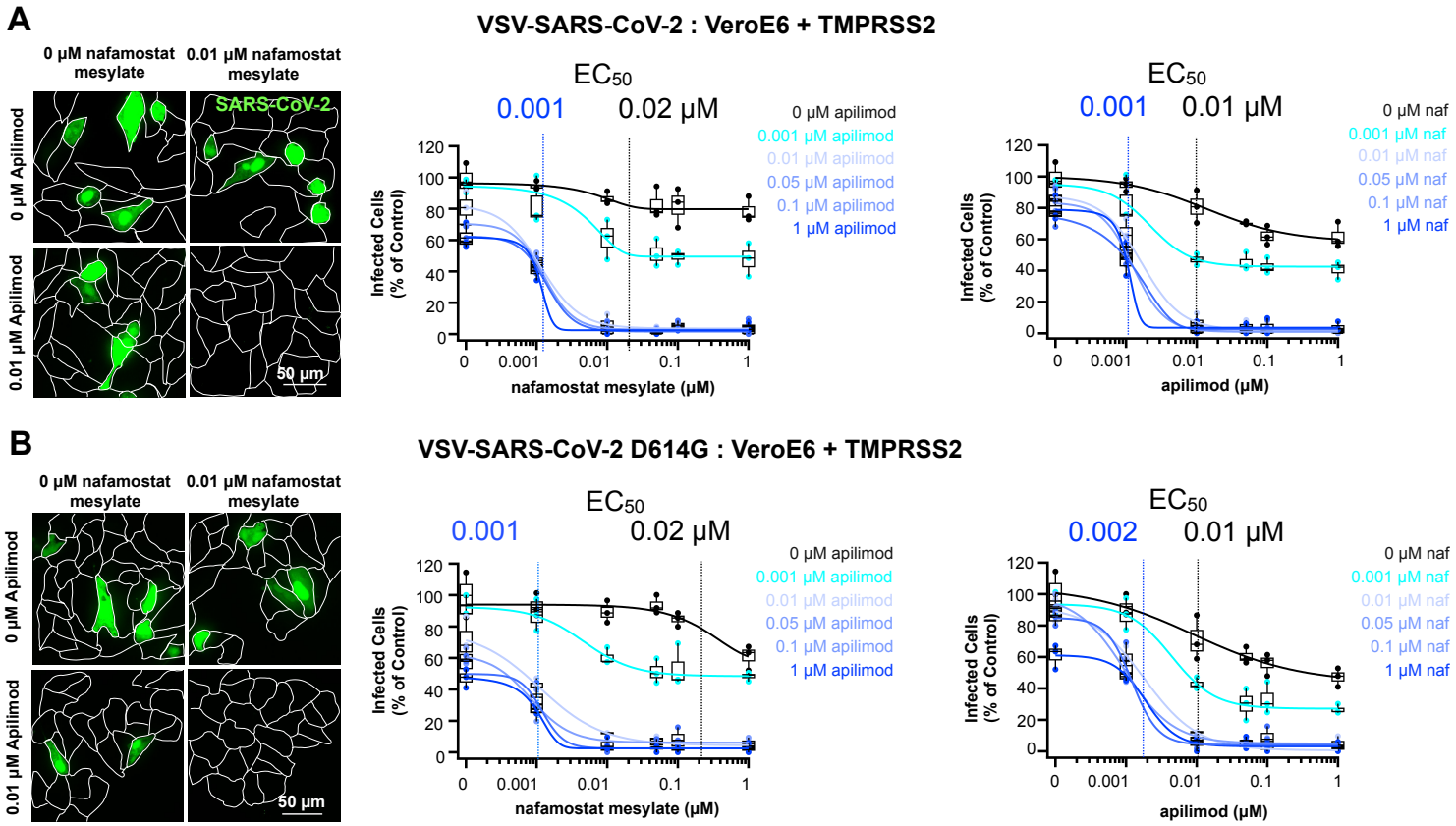
A
0 µM nafamostat mesylate
0.01 µM nafamostat mesylate
0 µM Apilimod
0.01 µM Apilimod
SARS-CoV-2
50 µm
VSV-SARS-CoV-2 : VeroE6 + TMPRSS2
EC50
0.001
0.02 µM
0 µM apilimod
0.001 µM apilimod
0.01 µM apilimod
0.05 µM apilimod
0.1 µM apilimod
1 µM apilimod
Infected Cells (% of Control)
nafamostat mesylate (µM)
EC50
0.001
0.01 µM
0 µM naf
0.001 µM naf
0.01 µM naf
0.05 µM naf
0.1 µM naf
1 µM naf
apilimod (µM)
B
VSV-SARS-CoV-2 D614G : VeroE6 + TMPRSS2
EC50
0.001
0.02 µM
EC50
0.002
0.01 µM
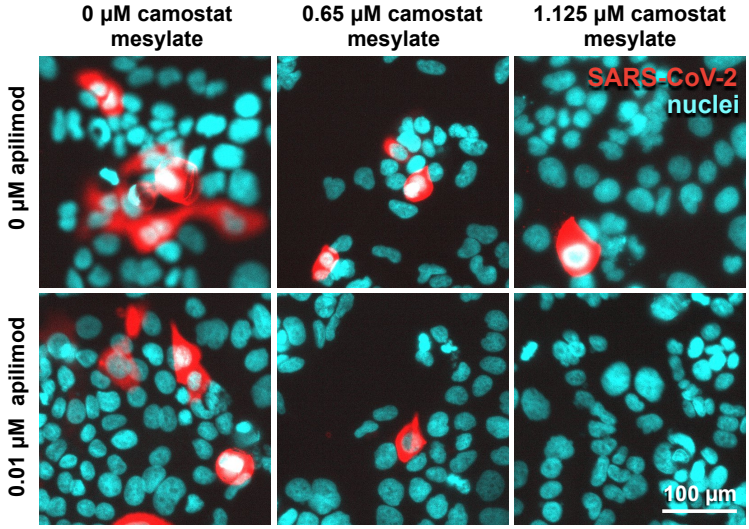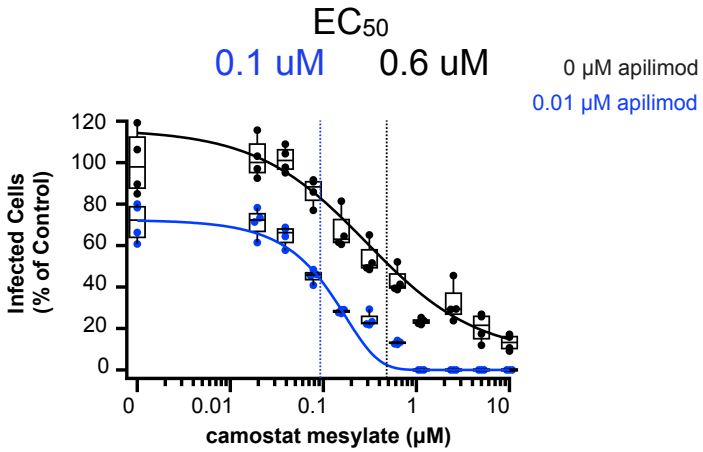
SARS-CoV-2 : Caco-2 + hACE2